Primitive Path Identification and Entanglement Statistics in Polymer Melts: Results from Direct Topological Analysis on Atomistic Polyethylene Models

ARTICLE *in* MACROMOLECULES · JUNE 2006

Impact Factor: 5.8 · DOI: 10.1021/ma060306b

4 AUTHORS, INCLUDING:

Martin Kröger
ETH Zurich
239 PUBLICATIONS **3,828** CITATIONS

SEE PROFILE

Primitive Path Identification and Entanglement Statistics in Polymer Melts: Results from Direct Topological Analysis on Atomistic Polyethylene Models

Katerina Foteinopoulou, Nikos Ch. Karayiannis, and Vlasis G. Mavrantzas

Department of Chemical Engineering, University of Patras, Patras GR 26504, Greece, and Institute of Chemical Engineering and High-Temperature Chemical Processes, FORTH-ICE/HT, Patras GR 26504, Greece

Martin Kröger*

Polymer Physics, ETH Zürich, Department of Materials, Wolfgang-Pauli-Str. 10, CH-8093 Zürich, Switzerland

Received February 9, 2006; Revised Manuscript Received March 29, 2006

ABSTRACT: A large number of well-equilibrated atomistic configurations of linear, strictly monodisperse polyethylene (PE) melts of molecular length ranging from C_{24} up to C_{1000}, obtained through extensive Monte Carlo simulations based on chain connectivity altering algorithms, have been subjected to a detailed topological analysis. Primitive paths are geometrically constructed connecting the two ends of a polymer chain (which in all cases are considered as fixed in space) under the constraint of no chain crossability, such that the multiple disconnected (coarse-grained) path has minimum contour length. When applied to a given, dense polymer configuration in 3-D space, the algorithm returns the primitive path (PP) and the related number and positions of entanglements (kinks) for all chains in the simulation box, thus providing extremely useful information for the topological structure (the primitive path network) hidden in bulk PE. In particular, our analysis demonstrates that once a characteristic chain length value (around C_{200}) is exceeded, the entanglement molecular length for PE at $T = 450$ K reaches a plateau value, characteristic of the entangled polymeric behavior. We further validate recent analytical predictions [Schieber, J. D. *J. Chem. Phys.* **2003**, *118*, 5162] about the shape of the distribution for the number of strands in a chain at equilibrium. At the same time, we show that the number of entanglements obtained by assuming random walk statistics [Everaers, R. et al. *Science* **2004**, *303*, 823] deviates significantly from these predictions, which we regard as a clear evidence that by directly counting the entanglements and their distribution functions, as proposed here, offers advantages for a quantitative analysis of the statistical nature of entanglements in polymeric systems.

I. Introduction

It has long been realized that in dense, many-chain polymeric systems, even if the excluded volume is zero, chain dynamics is highly influenced by "topological" constraints, referred to as entanglements, resulting from chain uncrossability. These intermolecular constraints give rise to "reptation"[1] dynamics that is nicely captured by the "tube" theory[2] and its numerous extensions and generalizations.[3−11] Although for polymeric systems consisting of chains with open ends there is no topological quantity to be discussed, algorithms have been proposed to characterize the entangled state, to extract a multiple disconnected path of either shortest contour length[12−15] or lowest energy,[16,17] to identify the corresponding primitive path (PP) (tube centerline), and to calculate the number of entanglements. As described in ref 13, entanglements effectively restrict individual chain conformations in a curvilinear tubelike region enclosing each chain. For very short time scales, chain segments are allowed to freely fluctuate in all directions until their displacements become commensurate with the tube diameter. Once the topological constraints are encountered, chain motion perpendicular to the primitive path is restricted and polymer segments diffuse along the PP. Doi−Edwards[2] define the PP as the shortest path connecting the two ends of the chain with the same topology as the chain itself relative to the surrounding obstacles.[1,2,7,16,18−20] From a mathematical point of view, the geometric procedure of extracting the primitive paths for a system filled with polymer chains has a unique solution only for the 2-D case. In the case of a 3-D simulation box, the solution of the PP identification is rigorous only when the primitive path of a single embedded chain is constructed by considering all other chain segments as fixed line obstacles.[21]

Methods have been developed in the past years for extracting the PP network simultaneously for all chains present in a simulation cell, yielding an optimum multiple disconnected path.[12−17,19,22] In the present work, a hierarchical modeling methodology is adopted: First, atomistic configurations of strictly monodisperse polyethylene (PE) melts are equilibrated at all length scales through extensive Monte Carlo (MC) simulations based on advanced chain connectivity altering algorithms. In the second stage, representative atomistic trajectories are mapped onto trajectories of primitive paths by employing a recently proposed geometric algorithm (the "Z-code").[12,19] According to this, the primitive paths, treated as "infinitely" thin and tensionless lines connecting the two ends of a polymer chain (which in all cases are considered as fixed in space[16,18,23]), are obtained under the constraint of chain uncrossability, such that the invoked geometric operations minimize (simultaneously for all chains present in the simulation cell) the contour length of the multiple disconnected path, i.e., the contour length summed over all individual PPs.[12,19] The algorithm returns a solution which is robust against minor displacements of the disconnected path and chain relabeling; it is also computationally efficient compared to dynamical mini-

* Corresponding author. E-mail: mk@mat.ethz.ch.

10.1021/ma060306b CCC: $33.50
Published on Web 05/13/2006

Table 1. Details of the Simulated Linear Monodisperse PE Melt Systems ($T = 450$ K, $P = 1$ atm)[a]

system	no. of chains	total MW [g/mol]	no. of configurations	CPU time [s] (original cell)	CPU time [s] (super-cell)
C_{24}	50	338	900	0.069	5.4
C_{34}	50	478	900	0.23	13
C_{48}	50	674	2800	0.25	41
C_{70}	80	982	3000	0.93	187
C_{78}	40	1094	2500	0.42	52
C_{100}	48	1402	6500	0.72	95
C_{122}	48	1710	6000	1.1	167
C_{142}	22	1990	7000	0.45	71
C_{174}	32	2438	4500	0.91	137
C_{224}	32	3138	7000	1.4	207
C_{270}	32	3782	10000	2.9	285
C_{320}	32	4482	7000	3.8	399
C_{400}	16	5602	5500	3.5	225
C_{500}	16	7002	7000	3.5	371
C_{1000}	8	14002	10000	3.7	634

[a] Also listed is the total number of different equilibrated configurations used in the topological analysis for each system and the average CPU time per frame for the original and super-sized simulation cells.

mization procedures used in refs 14−16. After identifying the PPs, the number of topological entanglements is simply obtained either by counting the interior kinks or from the average length of a line segment, to be denoted as $\check{Z}$ (hat-kinked) and $\tilde{Z}$ (tilde-coiled), respectively. Their averages over all PPs in the simulation box and over all (equilibrated) MC configurations analyzed will be denoted as $\langle\check{Z}\rangle$ and $\langle\tilde{Z}\rangle$; in the rest of the paper whether Z stands for either $\check{Z}$ or $\tilde{Z}$ will become obvious from the context. Besides these measures whose inter-relation will be discussed in detail below, the construction of the PP network will allow us to study a number of other important quantities (such as the tube diameter (a_{pp}), the entanglement length (N_e), the Kuhn step length (b_{pp}), and the contour length (L_{pp})) and their distributions. This information is required for the development of coarse-grained descriptors that should be embedded into a beyond-equilibrium thermodynamics framework in order to analyze the response of a polymer melt to an applied flow field.[24−26]

II. Methods

A. Molecular Model−Systems Studied−Monte Carlo Equilibration. All results to be presented in the next sections are obtained by applying the Z-code on strictly monodisperse linear PE melt configurations accumulated in the course of exhaustive atomistic equilibration simulations with the very efficient chain connectivity altering double-bridging Monte Carlo algorithm (DBMC).[27−29] Table 1 gives a summary of the molecular characteristics of the systems (chain length or molecular weight and total number of chains) equilibrated with DBMC and subsequently analyzed with the Z-code; it also reports the total number of independent (and fully equilibrated) configurations on which the algorithm is applied in order to get accurate predictions of the topological properties and the average computer processing unit (CPU) time per frame for the PP analysis of the original and super-sized (see discussion in section III.B) simulation cells. All reported CPU times correspond to serial runs on an Intel Xeon (Linux) workstation at 2.8 GHz with a 2 GB memory. Details of the simulation strategy employed to sample these configurations with the DBMC algorithm have been reported in a number of past publications and will be briefly discussed here.

All MC simulations are carried out with the united-atom (UA) molecular model,[27,28] which regards each CH_2 and CH_3 group as a single, spherically symmetric interacting site. The values of all bond lengths CH_x-CH_2 ($x \in \{2, 3\}$) are kept fixed at $l_0 = 1.54$ Å, while for the bond angles $CH_x-CH_2-CH_2$ ($x \in \{2, 3\}$), which are allowed to fluctuate harmonically around an equilibrium value of $\theta_0 = 114°$, the Van der Ploeg and Berendsen potential[30]

$$\frac{V_{bend}(\theta)}{k_B} = \frac{1}{2}k_\theta(\theta - \theta_0)^2 \tag{1}$$

is adopted with k_B the Boltzmann constant and $k_\theta = 62\,500$ K rad^{-2}. For all dihedral angles $CH_x-CH_2-CH_2-CH_2$ ($x \in \{2, 3\}$) the Toxvaerd's nine-term, sum of cosines torsional potential[31]

$$\frac{V_{tor}(\phi)}{k_B} = \sum_{i=0}^{8} c_i \cos^i(\phi) \tag{2}$$

is used with $c_{0-8} = (1001, 2130, -303, -3612, 227, 1966, -4489, -1736, 2817)$ K. As far as the nonbonded interactions are concerned, for all intramolecular pairs (i, j) of sites separated by more than three bonds and all intermolecular ones, a 12−6 Lennard-Jones potential

$$V_{L-J}(r_{ij}) = 4\epsilon_{ij}\left[\left(\frac{\sigma_{ij}}{r_{ij}}\right)^{12} - \left(\frac{\sigma_{ij}}{r_{ij}}\right)^{6}\right] \tag{3}$$

is implemented where r_{ij} is the distance between the sites and ϵ_{ij} ($\epsilon_{CH_2} = \epsilon_{CH_3} = 0.0914$ kcal/mol) and σ_{ij} ($\sigma_{CH_2} = \sigma_{CH_3} = 3.95$ Å) denote the well depth and collision diameter, respectively, of the TraPPE model.[32]

Initial configurations for the MC simulations are provided by the three-stage, constant-density energy minimization technique of Theodorou and Suter[33] (the molecular mechanics method, MM) with the density fixed at ∼0.77 g/cm^3 for all systems. The resulting minimum-energy configurations are then subjected to very long MC simulations with the DBMC algorithm,[27−29] in the isothermal−isobaric (NPT) statistical ensemble with the temperature and pressure set equal to $T = 450$ K and $P = 1$ atm, respectively. The following mix of moves is used in all simulations [percentages in parentheses denote attempt probabilities]: flips[34] (5%), end-mer rotations (3%), reptations[35] (15%), concerted rotations (ConRot's)[36] (20%), volume fluctuations (2%), double bridgings (DB's)[27−29] (30%), intramolecular double rebridgings (IDR's)[27−29] (10%), and intramolecular end bridgings (IEBs)[37] (15%). As suggested by previous MC simulations on PE oligomers, for systems characterized by small chain lengths ($<C_{70}$) the portion of IDR is reallocated to DB to increase the equilibration efficiency of the algorithm.[28] Configurations are recorded every 2×10^5 MC steps so that the corresponding atomistic trajectories consist of a large number (on the order of a few thousands) of fully equilibrated, statistically independent configurations. It is with these configurations that all results of the present topological analysis have been obtained.

B. Primitive Path Network. The Z-code algorithm, adopted in the topological analysis, solves the problem of the shortest multiple disconnected path in the sense of minimum Euclidean length subject to constraints arising from the initial state.[12,19] This method is efficient to extract entanglements from physical (atomistic) configurations by translating the physical problem based on the Doi−Edwards concept[2] into a corresponding mathematical problem, providing an approximate but model independent and efficiently obtained solution. In contrast to previous efforts, this direct geometric procedure[12,19] minimizes the total PP length and not the total (reweighted physical interaction) energy of the system subject to an artificial external

field.[16] Neighbor lists are used to identify all candidate intersecting segments of intermolecular origin, and periodic boundary conditions are applied in all dimensions. A finite thickness threshold is incorporated so as to ensure that no entanglements are missed from the geometric tracking due to the finite representation of numbers. As soon as the minimization procedure converges, the number of interior kinks (entanglements) for each chain, explicitly deduced from the shortest path, is quite insensitive to the exact conformation of the shortest path.[12] If N_{ch} is the number of chains in the simulation box, the code returns the same number (N_{ch}) of primitive paths along with the number and coordinates of kinks (entanglements) for them. Given a PP conformation as obtained through the application of Z-code on the original atomistic configuration, we calculate a set of related quantities such as the contour length L_{pp} of the shortest path and the number of interior nodes $\check{Z}$ for each PP, the latter being identified with the number of entanglements per chain. The contour length L_{pp} is derived directly from the PP configuration when the Z-code has converged and the minimization procedure has finished. For a given chain (consisting of N carbon atoms), given the number Z of entanglements, the entanglement length (number of carbon atoms between entanglements), N_e, can also be calculated through[16]

$$N_e = \frac{N}{Z + \frac{N}{N-1}} \tag{4}$$

where we follow the "Graessley/Fetters" definition of N_e[38] (reasons to include an additional factor of $^4/_5$ are thoroughly discussed in ref 39) and where the correction term $N/(N-1)$ is used to capture the limit: $Z = 0$ when $N_e = N - 1$. Equation 4 holds for $Z = \check{Z}$ and $N_e = \check{N}_e$, but also for the quantities $\tilde{Z}$ and $\tilde{N}_e$ to be introduced just below. Regarding the identification of the number of kinks per chain (and consequently the calculation of N_e from eq 4), we follow throughout the paper the original approach of ref 12 according to which kinks may occur in a single form or as pairs depending on the relative local configuration of the participating PPs. Several alternate definitions are, of course, possible.

In refs 16, 17, and 22, a way of calculating the number of entanglements per chain (and, consequently, the entanglement length) was introduced which makes use of the PP contour length L_{pp} and the square end-to-end distance R^2 of the chain (which remains unaltered during the minimization method as the resulting PP is derived under the constraint of fixed ends). The entanglement length, $\tilde{N}_e$, is calculated from the molecular length (the number of carbon atoms), N, of the original, atomistic chain, through[2]

$$\tilde{N}_e = \frac{a_{pp}}{b_{pp}} \tag{5}$$

where a_{pp} is obtained from

$$a_{pp} = R^2/L_{pp} \tag{6}$$

and b_{pp} the (assumed) constant step length of the primitive path, which, under the assumption that it forms a Gaussian coil, is given by

$$b_{pp} = \frac{L_{pp}}{N-1} \tag{7}$$

Using eqs 4 and 5 and the above definitions for a_{pp} and b_{pp}, the number of entanglements $\tilde{Z}$ of a chain containing N atoms and whose end-to-end distance is equal to R and its corresponding PP has a contour length equal to L_{pp} is given by

$$\tilde{Z} = \left(\frac{N}{N-1}\right)\left(\frac{L_{pp}^2}{R^2} - 1\right) \tag{8}$$

Equation 8 has been obtained under the assumption that the shortest path is a random path of equidistant step length. As will be shown in section 3.2, this is not the case, and correspondingly, the number of entanglements according to eq 8, $\tilde{Z}$, does not coincide with the number of entanglements $\check{Z}$ based on the (direct) identification of the interior nodes (kinks) of the PP. In general, $\tilde{Z}$ is a less accurate measure of the number of entanglements than $\check{Z}$, since it involves severe assumptions which can also fail in a dramatic fashion, as for example in a strong flow.[40,41] Most evidence for the differences between $\tilde{Z}$ and $\check{Z}$ will be provided in section III.B where the distributions $p(\check{Z})$ and $p(\tilde{Z})$ of the number of entangled strands, respectively, will be compared with each other. To clarify notation, p does not represent a unique function but stands for "probability density function" or "probability distribution" and depends on its argument. In section III.B, we will show that $p(\check{Z})$ coincides with the form derived in refs 26 and 42 while $p(\tilde{Z})$ does not.

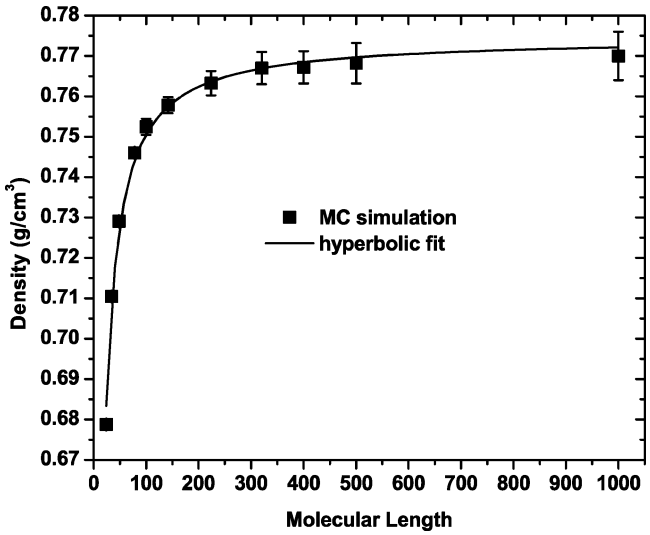

Figure 1. Density, ρ, as a function of molecular length, N, as obtained from the present MC simulations on monodisperse linear PE melts at $T = 450$ K and $P = 1$ atm. Also shown is the corresponding best fit to the simulation data using the hyperbolic expression of eq 9.

III. Results

A. Density and Chain Dimensions of the Simulated Atomistic PE Models. Figure 1 shows the density, ρ, of the simulated PE systems as a function of their molecular length, N, as obtained from the present MC simulations ($T = 450$ K, $P = 1$ atm). As has already been reported,[43] simulation data for the density can be accurately fitted with a hyperbolic function of the form

$$\rho(N,T,P) = \frac{\rho_\infty(T,P)}{1 + a_0(T,P)/N} \tag{9}$$

where $\rho_\infty(T,P)$ denotes the density at infinite molecular weight (MW) and $a_0(T,P)$ is a dimensionless constant describing the rate with which ρ increases with N. The best-fit values are a_0-(450 K, 1 atm) = 3.20 and ρ_∞(450 K, 1 atm) = 0.775 g/cm^3; the latter is in excellent agreement with the experimentally

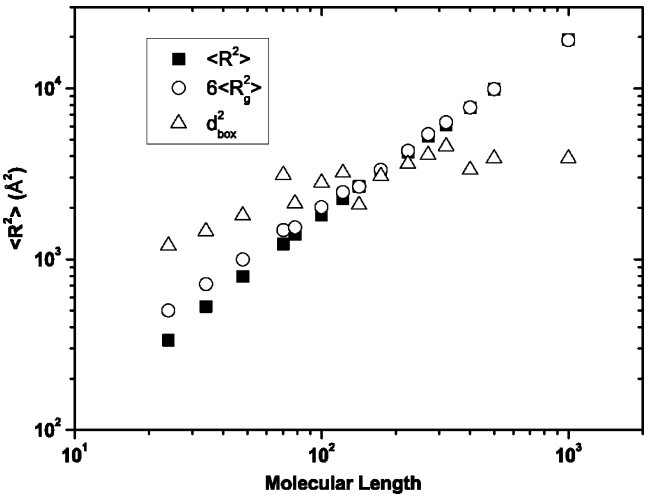

Figure 2. Mean-squared chain end-to-end distance, $\langle R^2 \rangle$, and mean-squared chain radius of gyration multiplied by a factor of 6, $6\langle R_g^2 \rangle$, as functions of molecular length, N, in logarithmic coordinates. Also shown for comparison is the mean-squared dimensions, d_{box}^2, of the simulation cell.

reported density value for infinitely long PE,[44] which is $\rho_{exp} = 0.766$ g/cm^3. On the basis of the volumetric data of Figure 1, all PE systems with chain length $C_{N\geq 224}$ are characterized by very similar density values indicative of a true polymeric behavior.

Figure 2 presents the dependence of the mean-square chain end-to-end distance, $\langle R^2 \rangle$, and the mean-square chain radius of gyration multiplied by six, $6\langle R_g^2 \rangle$, as a function of chain length and how they compare with the mean-square dimensions of the simulation box (i.e., with d_{box}^2), in logarithmic coordinates. Beyond approximately $C_{N\geq 142}$, $\langle R^2 \rangle = 6\langle R_g^2 \rangle$ for all simulated PE systems, in accord with Flory's random coil hypothesis for long-chain macromolecules.[45] At the chosen temperature and pressure conditions ($T = 450$ K, $P = 1$ atm), we recover recently obtained known[28] values of $\langle R^2 \rangle = (N-1)\, b^2 = (N-1)\, C_\infty l_0^2$, with $C_\infty = 8.27 \pm 0.15$, bond length $l_0 = 1.54$ Å, and $b \approx 4.42$ Å. In addition, from Figure 2 it is apparent that for PE systems with chain length greater than about C_{142}, the size of the simulation box becomes comparable to the chain dimensions. For even longer molecules, the mean value of the chain end-to-end distance significantly exceeds the box size; to cope with this, we thus had to artificially enlarge the parent cell (by 27 times, by introducing clone boxes along its x, y, and z directions).

B. Results from Primitive Path Analysis. We applied the shortest path algorithm (the Z-code[12]) with line thickness 10^{-7} Å to all systems listed in Table 1. The reduction of atomistically detailed chains to primitive paths (see, e.g., Figure 3) is performed simultaneously for all chains in the simulation box. Selected PPs along with their parent atomistic configurations are shown in Figure 4. As mentioned above, the Z-code should ideally be applied to polymer chain melts whose dimensions (as quantified by the mean chain radius of gyration) are significantly smaller than the dimensions of the simulation box, as the geometric procedure works optimally when the kink-to-kink distance is smaller than half of the simulation box size.

In addition, the algorithm we use does not identify self (intrachain)-entanglements. Besides the fact that there exists no unique definition of self-entanglements, the density of local self-knots has been quantified as being very small compared to that of the multichain (intermolecular) entanglements.[17] Thus, to quantify and then get rid of possible finite-size effects in the topological analysis, we artificially enlarged our originally

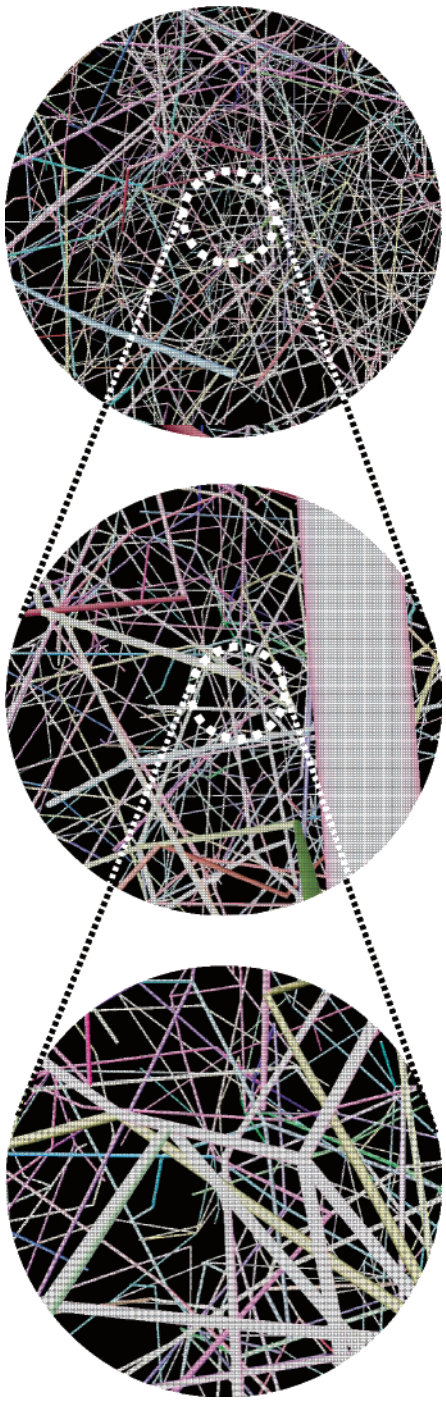

Figure 3. From top to bottom: zoom into the primitive path network (shortest multiple disconnected path)[12,13] as obtained from atomistic coordinates for a representative C_{500} system. Each chain has its own color. The thick bar in the central figure is a line segment closely passed by our camera and should leave a "dynamic" impression of the short sequence.

generated MC configurations to "super-boxes" (replicas) of volume (d_{box}^3) $3^3 = 27$ times larger than the original system size. Results from these calculations (in the form of percentage differences) about the contour length $\langle L_{pp} \rangle$, the entanglement length $\langle \check{N}_e \rangle$, the number of kinks (entanglements) $\langle \check{Z} \rangle$, and the step length $\langle a_{pp} \rangle$ are reported in Figure 5. As expected, the PP analysis for simulation boxes bearing longer PE chains (i.e., boxes whose size is rather small compared to the average chain dimension) underestimates $\langle \check{Z} \rangle$ and, consequently, overestimates $\langle \check{N}_e \rangle$. The effect is more pronounced for the smaller size systems of the longer chain molecules (e.g., for the 8-chain C_{1000} PE

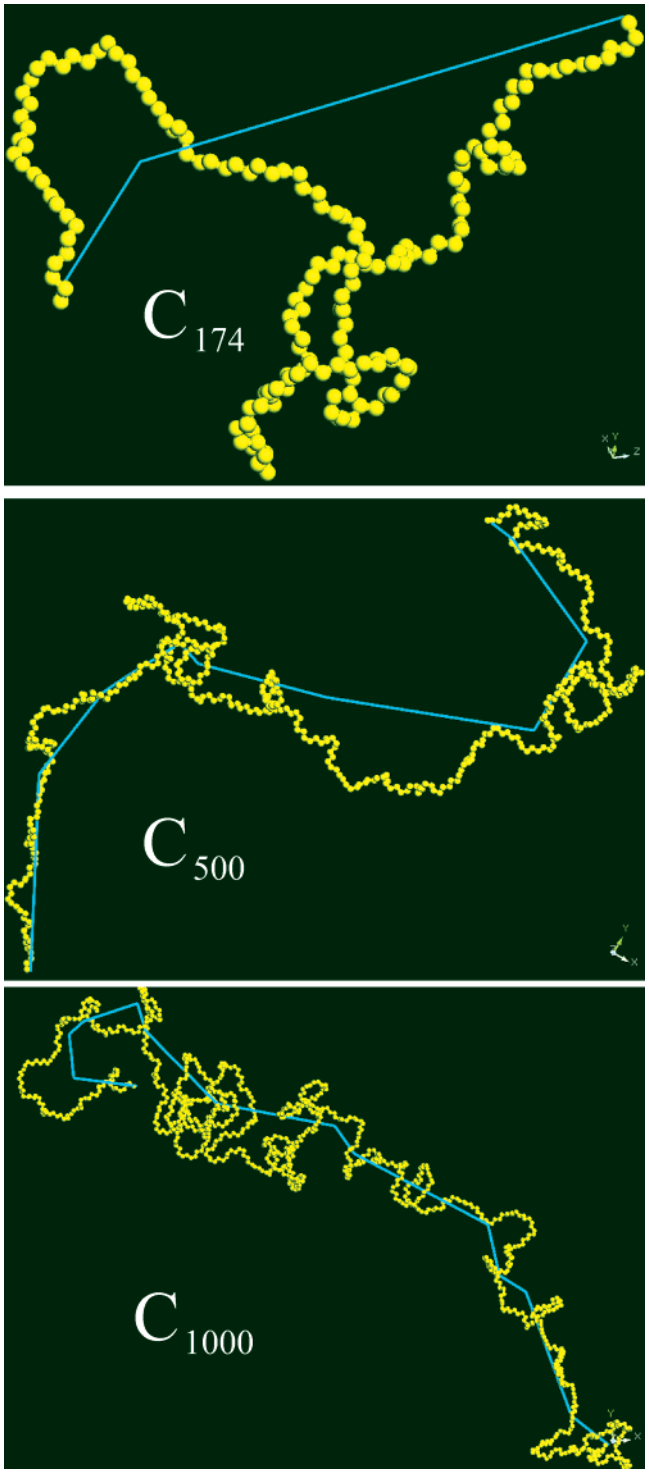

Figure 4. Illustration of the transformation of a selected atomistic chain to its primitive path for: (top) a C_{174}, (middle) a C_{500}, and (bottom) a C_{1000} PE molecule (in unwrap coordinates). The methyl units of the atomistic representation are marked in red (or dark gray) while those of the corresponding PP in blue (light gray). A many-chain system is shown in Figure 3.

melt). Figure 5 shows that the difference observed in the calculation of $\langle \check{N}_e \rangle$ from the original and artificially enlarged simulation boxes is negligible (around 5%) for the shorter PE systems ($C_{N<142}$) but quite significant (up to 30%) for the longer ones whose mean radius of gyration is commensurate with (or larger than) the box dimensions. The huge finite-size effect on results obtained with the original Z-code is a consequence of the particular implementation of neighbor cells in the Z-code

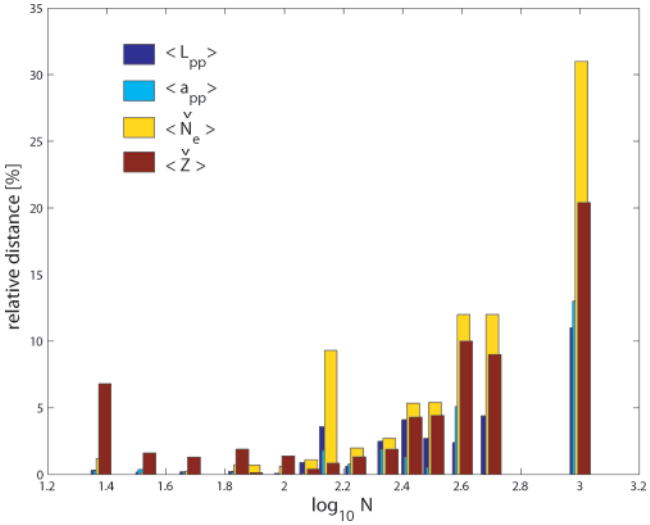

Figure 5. Percentage differences in contour length $\langle L_{pp} \rangle$, step length $\langle a_{pp} \rangle$, entanglement molecular length $\langle \check{N}_e \rangle$, and number of entanglements $\langle \check{Z} \rangle$ as a function of the logarithm of the molecular length N, when the PP analysis is applied on simulated systems with either ordinary or super-sized boxes, computed as $100|(Q^{\text{super-sized}} - Q^{\text{original}})/Q^{\text{super-sized}}|$ where Q denotes any of the above quantities.

and has been resolved at the time this paper went into press (see "Note Added in Proof", section IV).

All results reported in the following have been obtained by applying the Z-code on super-box systems, by averaging also over a large number of equilibrated configurations (on the order of a few thousands; see Table 1). For example, Figure 6 shows results for the instantaneous values of $\langle \check{Z} \rangle$, $\langle \check{N}_e \rangle$, $\langle \tilde{N}_e \rangle$, $\langle a_{pp} \rangle$, $\langle b_{pp} \rangle$, and $\langle L_{pp} \rangle$, still averaged over all chains in each configuration, for the C_{1000} PE system. According to Figure 6, to accurately estimate the mean entanglement length $\langle \check{N}_e \rangle$, averaging over a large number (close to 1500) of different PE configurations is definitely needed, revealing the impact of the equilibration procedure of the atomistic reference samples on the quality of the extracted data, as has also been identified in a previous work.[46] Although such configurations are easily provided here by our chain-connectivity altering MC algorithm,[27−29,43,47] it would be clearly impossible to sample them from a brute-force application of the conventional molecular dynamics (MD) method. We also repeat here that expressions 1−8 are used to obtain the above quantities for each chain at a given configuration and are subsequently averaged over all chains and all configurations (MC frames).

The dependence of the quantities $\langle \check{Z} \rangle$, $\langle \check{N}_e \rangle$, $\langle \tilde{N}_e \rangle$, $\langle L_{pp} \rangle$, $\langle b_{pp} \rangle$, and $\langle a_{pp} \rangle$ on chain molecular length is given in Figures 7−9. For long PE melts, the average number of entanglements per chain $\langle Z \rangle$ in Figure 7 comes out to be a linear function of the molecular length of the simulated system. It is also interesting to note that the shortest-path analysis suggests the existence of topological constraints or entanglements even for the shorter PE systems, such as the C_{48} PE oligomer, consistent with findings from recent atomistic MD simulations.[48]

Figure 8 presents the dependence of the average molecular length between entanglements (i.e., the entanglement spacing), $\langle \check{N}_e \rangle$, on the molecular length of the simulated PE systems. Data from monodisperse samples suggest that, once a characteristic chain length value (close to C_{200}) is exceeded, $\langle \check{N}_e \rangle$ reaches a plateau value characteristic of an entangled polymeric behavior. This finding is also consistent with our MD-based identification of reptation dynamics for systems characterized by an average chain length N greater than about C_{174}.[48] The average value of the entanglement spacing is calculated here to be equal to $\langle \check{N}_e \rangle$

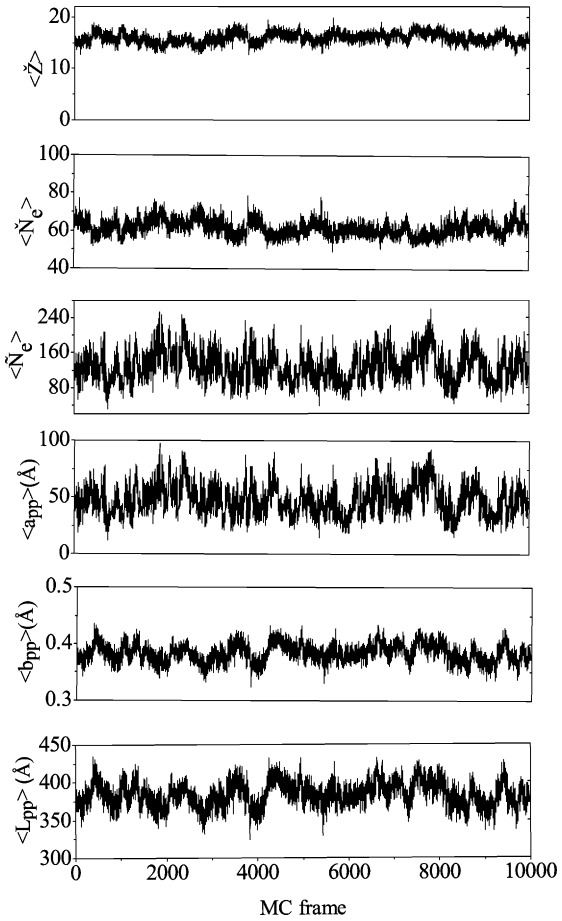

Figure 6. Variation of several quantities characterizing the PP network with MC frame in the course of the PP analysis with the C_{1000} PE melt. The values of the quantities shown in the figure have been obtained by averaging over all chains in the given MC frame (configuration). From top to bottom: Number of entanglements (kinks) $\langle \check{Z} \rangle$, entanglement length (number of carbon atoms) from kinks $\langle \check{N}_e \rangle$ or coils $\langle \tilde{N}_e \rangle$, step length $\langle a_{pp} \rangle$, Kuhn step length $\langle b_{pp} \rangle$, and contour length $\langle L_{pp} \rangle$ as defined in section II.B (see also section IV).

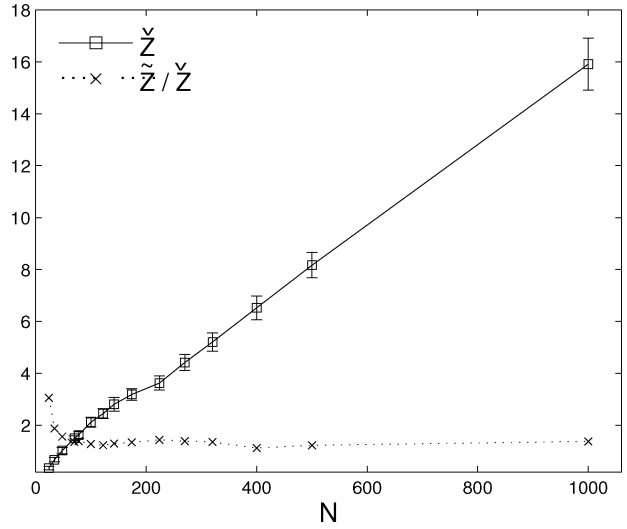

Figure 7. Average number of entanglements from kinks $\langle \check{Z} \rangle$ or coils $\langle \tilde{Z} \rangle / \langle \check{Z} \rangle$ vs molecular length N as obtained by applying the shortest-path analysis on model monodisperse PE melt systems ($T = 450$ K, $P = 1$ atm). At large N the number of entanglements is proportional to N and the ratio $\langle \tilde{Z} \rangle / \langle \check{Z} \rangle = 1.35 \pm 0.15$ (see also section IV).

$= 61 \pm 4$ (see section IV). This plateau value was further tested by applying the Z-code also on a very large system containing 64 chains of C_{1000} equilibrated through MC simulation directly from the beginning, that is, without artificially enlarging the 8-chain one as was done above. The value of the calculated entanglement spacing came out to be $\langle \check{N}_e \rangle = 60 \pm 6$, i.e., in perfect agreement with the results of the PP analysis on the super-sized systems obtained by artificially enlarging the smaller (original) ones. For comparison, Fetters et al.[49] propose an experimental value of $N_e \approx 82$ as calculated from the plateau modulus of the PE in the melt state ($T = 443$ K).

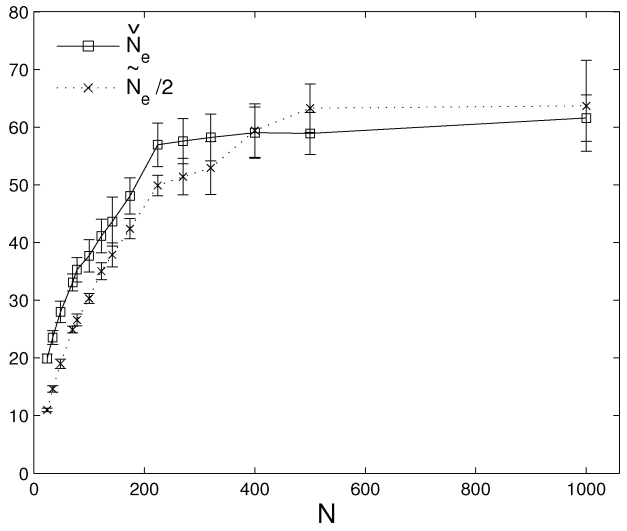

Figure 8. Average entanglement spacing (in carbon atoms) from kinks $\langle \check{N}_e \rangle$ or coils $\langle \tilde{N}_e/2 \rangle$ vs molecular length N as obtained by applying the shortest-path analysis on the atomistically detailed PE model systems. Differences between $\check{N}_e$ and $\tilde{N}_e$ arise due to (i) the very different shapes of the $p(\check{Z})$ and $p(\tilde{Z})$ distribution functions (cf. Figures 10 and 14) and (ii) the random walk assumption used to define $\tilde{N}_e$ as discussed in the main text (see also section IV).

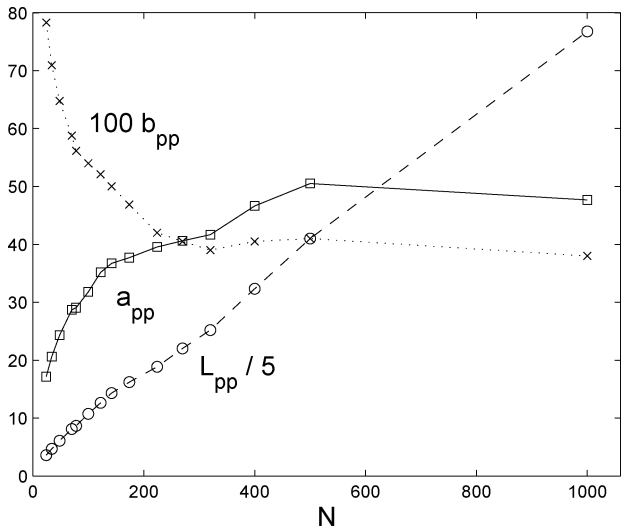

Figure 9. Scaled average contour length of the primitive paths $\langle L_{pp} \rangle$, average step length $\langle a_{pp} \rangle$, and average Kuhn length $\langle b_{pp} \rangle$ (all quantities given in Å) as a function of molecular length as obtained by applying the shortest-path analysis on the atomistically detailed PE melt configurations.

The shortest path contains much more detailed and valuable information about the coarse-grained variables of the entanglement network than just the above-mentioned averaged quantities. The equilibrium distribution of the number of entanglements, $p(\check{Z})$, which is readily available from the Z-code, contains useful information about the Z dependence of the free energy in a coarse-grained description. The $\check{Z}$ distribution, as computed directly from the number of kinks of the primitive paths, eq 4, for the C_{100}, C_{224}, C_{320}, C_{500}, and C_{1000} PE systems, is shown

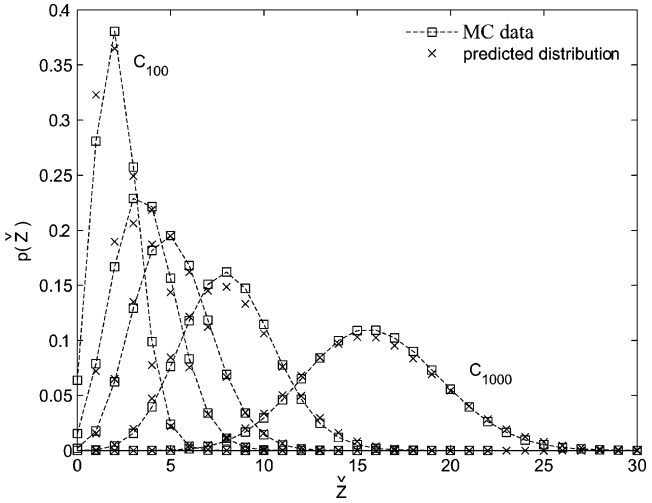

Figure 10. Distribution of the number of entanglements $\check{Z}$ as computed from the number of kinks of the primitive paths for the C_{100}, C_{224}, C_{320}, C_{500}, and C_{1000} PE systems. Also shown are the expected, parameter-free distribution functions according to eq A3 of the Appendix; the similarity with the simulation data is striking. For a quantitative comparison, see Table 2.

Table 2. Quantitative Comparison between the Present Simulation Data for $p(\check{Z})$ and the Analytical ("Parameter-Free") Distribution Function $p(Z)$ (of Eq A3)[a]

C_N	$\langle Z\rangle$	$\langle Z^2\rangle$	Δ^2 (%)	$\langle Z^3\rangle$	Δ^3 (%)	$\langle Z^4\rangle$	Δ^4 (%)
C_{100}	2.13	5.83	2.9	18.6	3.3	67	5.9
C_{224}	3.63	15.96	0.9	79.7	0.7	439	0.2
C_{320}	5.16	30.7	0.3	202.8	1.4	1463	3.2
C_{500}	8.17	72.9	1.4	700.3	3.9	7161	7.3
C_{1000}	15.90	266.1	0.7	4652.9	2.1	84733	4.0

[a] The table provides a quantitative measure of the agreement between the present simulation data and the analytical theory for the corresponding distribution function based on the expected values for three moments $\langle Z^\kappa\rangle = \sum_{Z=0}^{\infty} Z^\kappa p(Z)$, $\kappa = 2$, 3, and 4, of the distribution, together with the relative distance between predicted, eq A6, and measured quantities, $\Delta^\kappa \equiv |(\langle Z^\kappa\rangle_{\text{theory}} - \langle Z^\kappa\rangle)/\langle Z^\kappa\rangle_{\text{theory}}|$.

in Figure 10. Schieber,[26,42] by assigning the effect of the "tube" at each topological constraint (entanglement) through the use of a chemical potential bath for $\check{Z}$, predicts a Poisson distribution for the number of entanglements (see for example eq 8 in ref 26 and eq A3 in Appendix A). The parameter-free, expected distribution functions according to eq A3 of Appendix A, based on the original concept by Schieber, are also shown in Figure 10. The theoretical predictions of eq A3 are compared against our data from the application of the Z-code on the atomistically detailed PE systems in Figure 10, and for all practical purposes, the two sets of data are seen to coincide. To the best of our knowledge, this is the first time that Schieber's theory[26,42] is directly verified from first principles (atomistic simulations). For a more quantitative comparison the reader can inspect Table 2, where Schieber's analytical theory and the predictions of the present work are compared at the level of the moments of the distribution function $p(\check{Z})$ (which are analytically derived in Appendix A).

Figure 11 shows the corresponding distribution $p(\check{N}_e)$ of the molecular length between entanglements as computed from $p(\check{Z})$ using eq 4, i.e., $p(\check{N}_e) = -p(\check{Z})\, d\check{Z}/d\check{N}_e$ with $p(\check{Z})$ taken from Figure 10. Figure 12, on the other hand, presents the distribution of the Kuhn step length b_{pp} of the primitive paths (see eq 7). Since $\langle R^2\rangle \propto (N-1)$, the distribution $p(L_{pp})$ of the contour lengths between entanglements has the same form as the distribution $p(b_{pp})$ of the Kuhn length but is shifted horizontally.

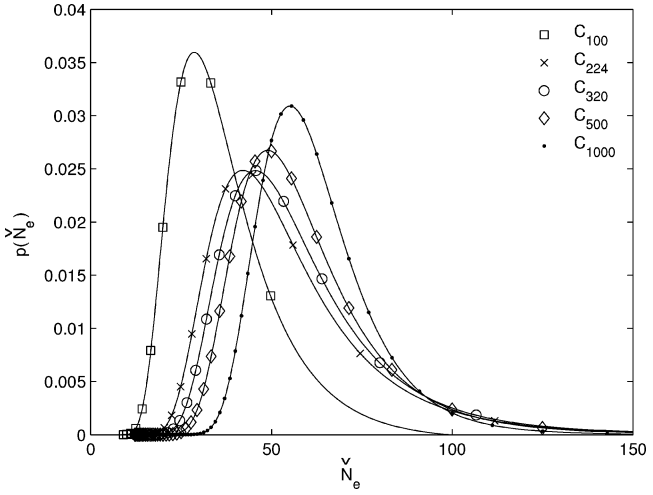

Figure 11. Distribution $p(\check{N}_e)$ of the chain length between entanglements $\check{N}_e$ as computed from $p(\check{Z})$ using eq 4, i.e., $p(\check{N}_e) = -p(\check{Z})d\check{Z}/d\check{N}_e$, with $p(\check{Z})$ taken from Figure 10.

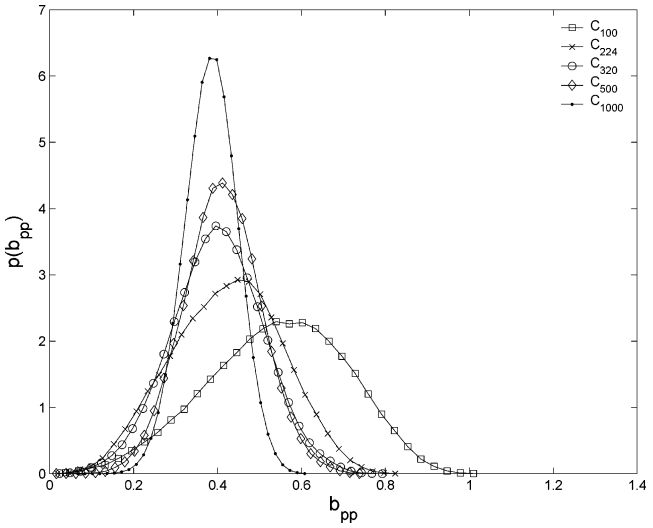

Figure 12. Distribution of the Kuhn step length of the primitive paths b_{pp} [given in Å], eq 7, as computed from the PP analysis for a number of PE systems.

In all cases investigated, the distribution $p(L_{pp})$ of the PP strand lengths is seen to follow a Gaussian distribution with a standard deviation that increases with increasing chain length. For the C_{1000} PE melt, for example, the standard deviation of the L_{pp} distribution function is so large that that the contour length of the primitive paths of some of the chains is shorter than for those in the C_{500} system, indicative of the strong fluctuations of the instantaneous shape of the atomistically detailed chains from the average coiled shape. To compare the present results for $p(L_{pp})$ with recent publications,[14] we chose to adopt the representation shown in Figure 13. The figure plots the scaled logarithm $-\ln[p(L_{pp})]/\langle\check{Z}\rangle$ of the distribution of contour lengths, $p(L_{pp})$, against the dimensionless contour length; also shown in the figure are the fits of the data with the "harmonic" expression[2,14] $p(L_{pp}) = p(\langle L_{pp}\rangle_0)\exp[-U(L_{pp})/k_BT]$, where $\langle L_{pp}\rangle_0$ is the most probable strand length, close to $\langle L_{pp}\rangle$, with $U(L_{pp}) = \nu\langle\check{Z}\rangle k_BT(L_{pp}/\langle L_{pp}\rangle_0 - 1)$.[2] Estimates of the parameter ν based on the theoretically calculated distribution $p(Z)$ of eq A3 are also available if we assume random walk statistics, as explained in Appendix A.

Figure 14 shows the distribution of the number of entanglements $\tilde{Z}$, where $\tilde{Z}$ is computed during the application of the shortest-path algorithm on atomistic MC configurations using

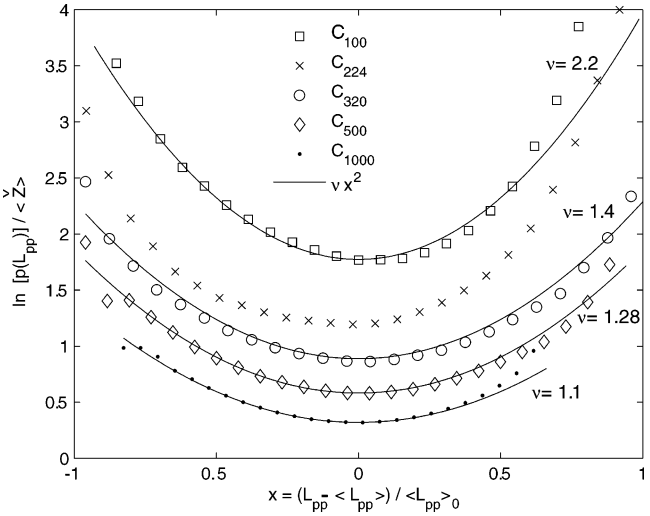

Figure 13. Scaled logarithm $-\ln[p(L_{pp})]/\langle\check{Z}\rangle$ of the distribution of contour lengths vs dimensionless contour length as computed from the PP analysis for a number of monodisperse PE systems at $T = 450$ K and $P = 1$ atm. Shown are results for the C_{100}, C_{224}, C_{320}, C_{500}, and C_{1000} PE systems together with fits to the "harmonic" expression[2,14] of $p(L_{pp}) \propto \exp[-U(L_{pp})/k_BT]$, with $U(L_{pp}) = \nu\langle\check{Z}\rangle k_BT(L_{pp}/\langle L_{pp}\rangle_0 - 1)^2$.

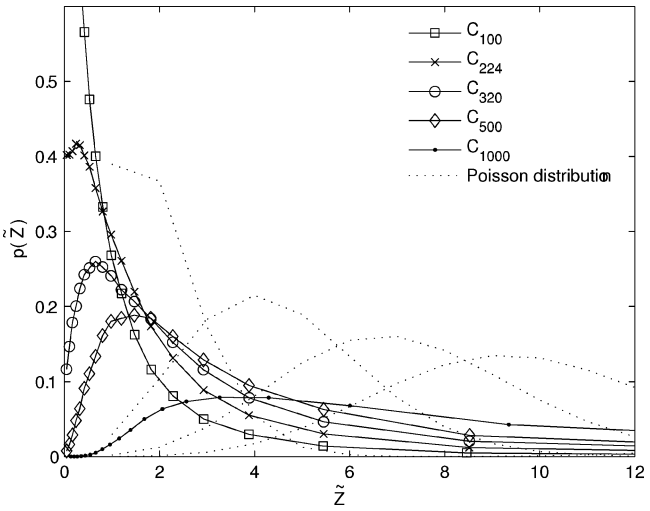

Figure 14. Distribution of the number of entanglements $\tilde{Z}$, where $\tilde{Z}$ is computed from the MC trajectories using eq 8, for the C_{224}, C_{320}, C_{500}, and C_{1000} PE systems. Large differences between the distribution $p(\tilde{Z})$ based on the implicit assumption of random path statistics and the one based on the direct identification and counting of kinks $p(\check{Z})$ (no such assumptions involved) are observed. Only the latter agrees with the expected Poisson shape (see, e.g., Figure 10).

eq 8 (assuming random walk), for the C_{224}, C_{320}, C_{500}, and C_{1000} systems. It also exemplifies the large differences recorded between theoretically calculated, eq A3, and atomistically extracted $p(\tilde{Z})$ functions. Clearly, significant deviations are observed between the distribution $p(\tilde{Z})$ based on the random walk picture and the distribution $p(\check{Z})$ based on the direct topological analysis and the identification of kink points. The latter is assumption-free, and it also agrees with the expected Poisson shape.[26,42] It therefore should be the preferred measure for future studies. However, it should be remembered that the quantities a_{pp} and b_{pp} have so far been defined only on the basis of Gaussian coil assumptions.

Figure 15 presents the distribution of step length a_{pp} of the constructed PPs as calculated through eq 6. For longer chain length systems (e.g., the C_{500} and C_{1000} ones), $p(a_{pp})$ is seen to follow a truncated-Gaussian function. It is also interesting to note that there are only tiny differences in the shape of the $p(a_{pp})$ distribution function for the C_{500} and C_{1000} systems. For both systems, the average value is $\langle a_{pp}\rangle = 48 \pm 11$ Å, which is in excellent agreement with the neutron-spin echo (NSE) measurements by Wischnewski et al.[50] at similar conditions ($T = 509$ K) which give a value of $a \approx 45$ Å for the step length. We should also note that the presently calculated value of the step length deviates from the value of $a = 32 \pm 2$ Å reported in our recent MD simulation study[48] through a calculation of the short-time behavior of segmental displacements by invoking an expression for a proposed by Likhtman−McLeish.[51]

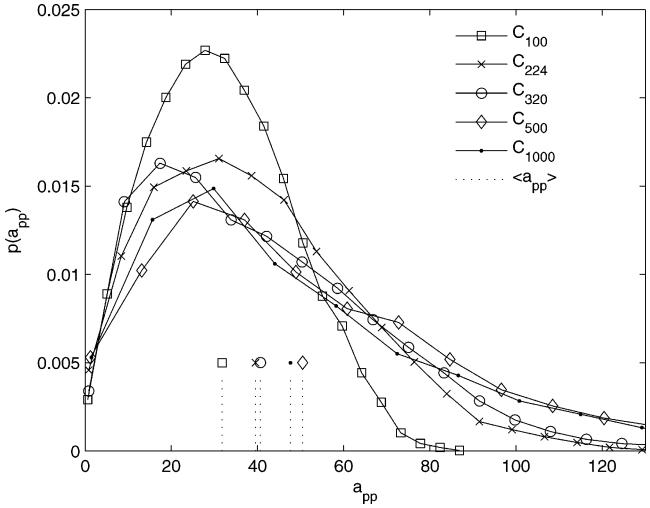

Figure 15. Distribution of step lengths, a_{pp} [Å], as computed from the PP analysis with the C_{100}, C_{224}, C_{320}, C_{500}, and C_{1000} PE systems.

IV. Summary and Conclusions

By suitably adapting the shortest-path algorithm (Z-code)[12,19] so that it can be applied to atomistically detailed model PE structures (accumulated in the course of long Monte Carlo simulations with the double-bridging algorithm[27−29]), we have been able to determine the equilibrium statistical properties of the primitive path network hidden in bulk PE melts.

The distribution of the number of entangled strands has been calculated from the shortest multiple disconnected path by (i) counting the number of kinks $\check{Z}$ and (ii) estimating the number of entanglements $\tilde{Z}$ from the contour length and the end-to-end distance of the PPs. We first recorded the expected[16,41,48,52] crossover between low- and high-molecular-weight polymeric behavior from the observed saturation in the variation of the number of carbon atoms between entanglements with chain length; this allowed us to determine the characteristic entanglement molecular weight based on the coarse-grained structure evaluated from the atomistic configurations. Second, we found that the distribution of the number of entanglements $\check{Z}$ (kinks) is practically identical to that predicted recently by Schieber.[26,42] The assumptions to be made to define $\tilde{Z}$ via eq 8 from the overall shape of the PPs were found to be inappropriate from a microscopic viewpoint. The PP is not a random walk with a constant step length, for which the conditional probability of having N_i monomers between PP nodes $i - 1$ and i with $i = 1, 2, ..., Z$ at a given number of entanglements Z can be written as $p(\{N_i\}, Z) \propto \delta(N - N_i Z)$. A more appropriate assumption seems to be that based on the use of statistical (combinatorial) weights, i.e., on the conditional probability $p(\{N_i\}, Z) \propto \delta(N - \sum_{i=1}^{Z} N_i)$ leading[42] to the binomial distribution $p(Z)$ given by eq A3 and observed in the present simulations. Notice also that eq A6 (for the relationship between the moments of the distribution $p(Z)$) seems to provide a rather convenient measure for characterizing

deviations from the equilibrium state (e.g., when a flow field is applied). The prefactors in the expression for the contour length potential, $U(L_{pp})$, have also been determined to be chain length dependent, which agrees with eq A3.

The (rather computationally inexpensive[12,19]) availability of the PPs and $p(\check{Z})$ from atomistic simulation offers a direct route of studying the dynamics of the primitive paths at and beyond equilibrium by explicitly taking into account the topological information; this should be contrasted with refs 4 and 52−54 where coarse-grained single-chain properties were used to analyze the dynamics and to compare against the reptation model. While single-chain properties in a polymer melt may reflect the statistics of the surrounding medium, this will not be the case in concentrated or dilute polymer systems for which (only) the direct many-chain topological approach will remain applicable.

Note Added in Proof. At the time this paper went into press, we finished developing an improved version of the Z-code, called Z1, which will be available to the public at http://www.complexfluids.ethz.ch/ within the research-tools section. Compared with the Z-code, Z1 is based on a different geometrical concept which makes the algorithm more robust against number precision deficiencies that we recovered lately, and does not require the use of "super-boxes" for (too small) systems prone to suffer from finite size effects. In addition, Z1 scales strictly with the number of particles (as a time step in molecular dynamics does), and it is, even for small systems, more efficient than the Z-code, while the Z-code already supersedes the efficiency of dynamical approaches by 2−3 orders of magnitude, and is running more efficiently than a related (Monte Carlo) approach "CReTA" implemented by Tzoumanekas and Theodorou.[13] From these recent investigations with Z1 we know that the value of the line thickness chosen here (10^{-7} Å) is too small and may easily reach limits due to finite number precision. Increasing this value to 10^{-4} Å in the Z-code results in qualitative changes in the values of L_{pp} (actually L_{pp} tends to increase) and of other related quantities ($\langle N_e\rangle$, $\langle a_{pp}\rangle$, $\langle b_{pp}\rangle$), but the shapes of the presented distributions and consequently the related discussions remain unaffected. The increase of the line thickness to 10^{-4} Å brings our results for L_{pp} in all studied systems very close to the ones obtained by Tzoumanekas and Theodorou through the "CReTA" algorithm applied on the same atomistic trajectories.[13] The revised plateau values are $\langle \check{N}_e\rangle = 43 \pm 2$, $\langle \tilde{N}_e\rangle = 87 \pm 20$, and $\langle a_{pp}\rangle = 40 \pm 8$ Å. Concerning $\langle \check{N}_e\rangle$, we should note that its absolute value as well as those of the related quantities are affected by the definition of kinks adopted in each topological algorithm: for example, in the Z-code two qualitative similar topological configurations may yield different number of kinks along the PP (see for example Figure 3 in ref 12), while in the "CReTA" algorithm kinks always occur as pairs (we refer the reader to ref 13 for more details). On the other hand, both the Z-code and the "CReTA" algorithms provide very similar predictions for quantities that are free from such ambiguities (i.e., L_{pp}, a_{pp}, and b_{pp}).

With an efficient geometrical implementation at hand, users will be in the position to investigate the dynamics of coarse-grained polymeric systems "on the fly", i.e., during a molecular dynamics run. The analysis of the PP network had so far been possible in a postprocessing step. On a modern single processor architecture, Z1 requires not more than 10^{-4} s of computing time per particle, which is roughly 2 orders of magnitude larger than the time needed to perform a single time step, i.e., the "on the fly" extraction of the coarse-grained representation of the polymer sample at every 1000 time steps (which, for entangled systems, is clearly sufficient in view of the slow relaxation of the PP network) will not effectively change the overall computing time of a hybrid code.

Acknowledgment. The Patras team is indebted to Dow Benelux B.V. and the Pythagoras II Programme (co-funded by the European Social Fund and National Resources) for financial support. We thank Prof. Doros Theodorou and Dr. Christos Tzoumanekas for very useful comments and for making their latest work available to us. This work was performed under the auspices of the EU-NSF program (project MNIBS, Contract No. FP6-016375) of the European Community and German Research Foundation (Priority Program 1104). The home organizations are thanked for the allocation of CPU time on their multiprocessor SGI workstation (origin, FORTH-ICE/HT) and linux cluster (gonzales, ETH Zurich).

Appendix. Equilibrium Distribution $p(Z)$

Unlike traditional network models, the number of Kuhn steps in an entangled strand has been treated by Schieber[26,42] as a dynamic, fluctuating quantity, rather than as a fixed parameter. Instead of putting the dangling ends in a chemical potential bath—analogous to the Maxwell demons of the tube model—Schieber ascribed the effect of the "tube" at each entanglement by using a chemical potential bath for the number of entanglements and then obtained a Poisson (equilibrium) distribution $P_\mu(n)$

$$p(Z) = P_\mu(n) \equiv \frac{\mu^n e^{-\mu}}{n!} \tag{A1}$$

with $n = (Z - 1)$, from an expression for the free energy (mainly a coarse-grained random walk). Notice that $\sum_{Z=0}^{N} p(Z) = 1$ for any positive integer N, and

$$\langle Z\rangle = \sum_{Z=0}^{N} Z p(Z) = \mu + 1 \tag{A2}$$

i.e., $\mu = \langle Z\rangle - 1 = \langle n\rangle \approx \langle N/N_e\rangle$ and more explicitly

$$p(Z) = \frac{\langle Z-1\rangle^{Z-1} e^{-\langle Z-1\rangle}}{(Z-1)!} \tag{A3}$$

For the second up to the fourth moments, eq A3 allows one to obtain the following expressions (written in terms of the first moment $\langle Z\rangle$ only):

$$\langle Z^2\rangle = \langle Z\rangle^2 + \langle Z\rangle - 1 \tag{A4}$$

$$\langle Z^3\rangle = \langle Z\rangle^3 + 3\langle Z\rangle^2 - 2\langle Z\rangle - 1 \tag{A5}$$

$$\langle Z^4\rangle = \langle Z\rangle^4 + 6\langle Z\rangle^3 + \langle Z\rangle^2 - 9\langle Z\rangle - 1 \tag{A6}$$

which help to decide if the measured $p(Z)$ coincides with that of eq A3 (without the need for any fitting parameters). For large Z, we can use Stirling's formula $Z! \approx \sqrt{2\pi Z}(Z/e)^Z$ to rewrite eq A3 as

$$p(Z) = \left(\frac{\langle Z-1\rangle}{Z-1}\right)^{Z-1} \frac{e^{Z-1-\langle Z-1\rangle}}{\sqrt{2\pi(Z-1)}} \tag{A7}$$

The distribution of eq A7 is closely related to that obtained by Rubinstein[55] using "reptons". From $p(Z)$ we can directly calculate the distribution of strand lengths $\tilde{p}(N_e)$ as

$$\tilde{p}(N_e) = -p(Z)\frac{dZ}{dN_e} = p\left(\frac{N}{Z + N/(N-1)}\right)\frac{N}{{N_e}^2} \quad \text{(A8)}$$

according to eq 4, for a given N, with p from eq A3. Equation A8 strictly holds for both pairs: $Z = \check{Z}$, $N_e = \check{N}_e$ and $Z = \tilde{Z}$, $N_e = \tilde{N}_e$. Using oversimplifying random walk statistics in a brutal manner, in particular by assuming that $R^2 = (N-1)\,b^2$ (for all N), we can also predict distribution functions based on eq A3 such as the one studied in ref 14, namely

$$\tilde{p}(L_{pp}) = p(\tilde{Z})\frac{d\tilde{Z}}{dL_{pp}} = p\left[\frac{N}{N-1}\left(\frac{{L_{pp}}^2}{R^2} - 1\right)\right]\frac{2N}{N-1}\frac{L_{pp}}{R^2} \quad \text{(A9)}$$

to obtain estimates of ν in the classical expression[2,14]

$$\tilde{p}(L_{pp}) = A\exp\left[-\nu\langle Z\rangle\left(\frac{L_{pp}}{\langle L_{pp}\rangle_0} - 1\right)^2\right], \quad A \approx \frac{\sqrt{\nu\langle Z\rangle/\pi}}{\langle L_{pp}\rangle_0} \quad \text{(A10)}$$

by simply evaluating the second derivative of $p(Z)$ with respect to Z at its maximum. Using $N_e = 60$, such a procedure for infinite chain length yields $\nu \approx 2$; in general, ν is a decreasing function of chain length. For example, $\nu \approx 2.6$ for $N = 500$, and $\nu \approx 3$ for $N = 300$, based on eq A3. Despite the oversimplifications made, these numbers are compatible with the observations made in ref 14 that $\nu = 2.9$ based on an energy minimization and $\nu = 1.4$ based on length minimization. Lower values of ν by roughly a factor of 2 (compared to the "expected" ones), e.g., $\nu < 2$, are observed in this work (see, e.g., Figure 13).

References and Notes

(1) De Gennes, P. G. *Macromolecules* **1976**, *9*, 587.
(2) Doi, M.; Edwards, S. F. *The Theory of Polymer Dynamics*; Clarendon: Oxford, 1986.
(3) Mead, D. W. *Macromolecules* **1998**, *31*, 7895.
(4) McLeish, T. C. B. *Adv. Phys.* **2002**, *51*, 1379.
(5) Marrucci, G.; Ianniruberto, G. *Macromolecules* **2004**, *37*, 3934.
(6) Wagner, M. H.; Kheirandish, S.; Hassager, O. *J. Rheol.* **2005**, *49*, 1317.
(7) Kröger, M. *Phys. Rep.* **2004**, *390*, 453.
(8) Marrucci, G. *Science* **2003**, *301*, 1681.
(9) Öttinger, H. C. *J. Non-Newtonian Fluid Mech.* **2000**, *89*, 165.
(10) Fang, J.; Kröger, M.; Öttinger, H. C. *J. Rheol.* **2000**, *44*, 1293 and references cited herein.
(11) Kröger, M. *Physica A* **1993**, *195*, 336.
(12) Kröger, M. *Comput. Phys. Commun.* **2005**, *168*, 209.
(13) Tzoumanekas, C.; Theodorou, D. N. cond-mat/0602555.
(14) Zhou, Q. Q.; Larson, R. G. *Macromolecules* **2005**, *38*, 5761.
(15) Shanbhag, S.; Larson, R. G. *Phys. Rev. Lett.* **2005**, *94*, 076001.
(16) Everaers, R.; Sukumaran, S. K.; Grest, G. S.; Svaneborg, C.; Sivasubramanian, A.; Kremer, K. *Science* **2004**, *303*, 823.
(17) Sukumaran, S. K.; Grest, G. S.; Kremer, K.; Everaers, R. *J. Polym. Sci., Part B: Polym. Phys.* **2005**, *43*, 917.
(18) Rubinstein, M.; Helfand, E. *J. Chem. Phys.* **1985**, *82*, 2477.
(19) Kröger, M. *Models for Polymeric and Anisotropic Liquids*; Lecture Notes in Physics 675; Springer: Berlin, 2005.
(20) Kröger, M.; Voigt, H. *Macromol. Theory Simul.* **1994**, *3*, 639.
(21) Sack, J.-R., Urrutia, J., Eds.; *Handbook of Computational Geometry*; Elsevier: Amsterdam, 2000; pp 633−701.
(22) Kremer, K.; Sukumaran, S. K.; Everaers, R.; Grest, G. S. *Comput. Phys. Commun.* **2005**, *169*, 75.
(23) Rouse, P. E. *J. Chem. Phys.* **1953**, *21*, 1272.
(24) Öttinger, H. C. *Beyond Equilibrium Thermodynamics*; Wiley: Hoboken, NJ, 2005.
(25) Öttinger, H. C. *Appl. Rheol.* **1999**, *9*, 17.
(26) Schieber, J. D. *J. Chem. Phys.* **2003**, *118*, 5162.
(27) Karayiannis, N. C.; Mavrantzas, V. G.; Theorodou, D. N. *Phys. Rev. Lett.* **2002**, *88*, 105503.
(28) Karayiannis, N. C.; Giannousaki, A. E.; Mavrantzas, V. G.; Theodorou, D. N. *J. Chem. Phys.* **2002**, *117*, 5465.
(29) Karayiannis, N. C.; Giannousaki, A. E.; Mavrantzas, V. G. *J. Chem. Phys.* **2003**, *118*, 2451.
(30) Van der Ploeg, P.; Berendsen, J. C. *J. Chem. Phys.* **1982**, *76*, 3271.
(31) Toxvaerd, S. *J. Chem. Phys.* **1997**, *107*, 5197.
(32) Martin, M. G.; Siepmann, J. I. *J. Phys. Chem. B* **1998**, *102*, 2569.
(33) Theodorou, D. N.; Suter, U. W. *Macromolecules* **1985**, *18*, 1467.
(34) Mavrantzas, V. G.; Theodorou, D. N. *Macromolecules* **1999**, *31*, 6310.
(35) Vacatello, M.; Avitabile, G.; Corradini, P.; Tuzi, A. *J. Chem. Phys.* **1980**, *73*, 548.
(36) Dodd, L. R.; Boone, T. D.; Theodorou, D. N. *Mol. Phys.* **1993**, *78*, 961.
(37) Karayiannis, N. C.; Daoulas, K. C.; Mavrantzas, V. G., to be submitted to *Macromolecules*.
(38) Fetters, L. J.; Lohse, D. J.; Richter, D.; Witten, T. A.; Zirkel, A. *Macromolecules* **1994**, *27*, 4639.
(39) Larson, R. G.; Sridhar, T.; Leal, L. G.; McKinley, G. H.; Likhtman, A. E.; McLeish, T. C. B. *J. Rheol.* **2003**, *47*, 809.
(40) Kröger, M.; Loose, W.; Hess, S. *J. Rheol.* **1993**, *37*, 1057.
(41) Kröger, M. *Phys. Rev. Lett.* **2000**, *85*, 1128.
(42) Schieber, J. D.; Neergaard, J.; Gupta, S. *J. Rheol.* **2003**, *47*, 213.
(43) Mavrantzas, V. G.; Boone, T. D.; Zervopoulou, E.; Theodorou, D. N. *Macromolecules* **1999**, *32*, 5072.
(44) Dee, G. T.; Ougizawa, T.; Walsh, D. J. *Polymer* **1992**, *33*, 3462.
(45) Flory, P. J. *Statistical Mechanics of Chain Molecules*; Wiley: New York, 1969.
(46) Hoy, R. S.; Robbins, M. O. *Phys. Rev. E* **2005**, *72*, 061802.
(47) Pant, P. V. K.; Theodorou, D. N. *Macromolecules* **1995**, *28*, 7224.
(48) Karayiannis, N. C.; Mavrantzas, V. G. *Macromolecules* **2005**, *38*, 8583.
(49) Fetters, L. J.; Lohse, D. J.; Milner, S. T.; Graessley, W. W. *Macromolecules* **1999**, *32*, 6847.
(50) Wischewski, A.; Monkenbush, M.; Willner, L.; Richter, D.; Likhtman, A. C.; McLeish, T. C. B., Farago, B. *Rhys. Rev. Lett.* **2002**, *88*, 058301.
(51) Likhtman, A. E.; McLeish, T. C. B. *Macromolecules* **2002,** *35*, 6332.
(52) Harmandaris, V. A.; Mavrantzas, V. G.; Theodorou, D. N.; Kröger, M.; Ramírez, J.; Öttinger, H. C.; Vlassopoulos, D. *Macromolecules* **2003**, *36*, 1376.
(53) Kremer, K.; Grest, G. S. *J. Chem. Phys.* **1990**, *92*, 5057.
(54) Kröger, M.; Ramírez, J.; Öttinger, H. C. *Polymer* **2002**, *43*, 477.
(55) Rubinstein, M. *Phys. Rev. Lett.* **1987**, *59*, 1946.

MA060306B